Improvement of a Non-Contact Elevator Guiding System by Implementation of an Additional Torsion Controller

Benedikt Schmülling, Peter Laumen, and Kay Hameyer
Institute of Electrical Machines, RWTH Aachen University,
Schinkelstraße 4, D-52056 Aachen, Germany
phone: (+49)-241-80-97667, fax: (+49)-241-80-92270
E-mail: Benedikt.Schmuelling@iem.rwth-aachen.de

***Abstract*— This paper describes the improvement of an electromagnetic elevator guiding system. Based on an existing system, which is able to control five spatial degrees of freedom of an elevator car, a system enhancement is proposed. The system of five controlled spatial degrees of freedom is augmented by a sixth degree of freedom: This is the elevator car's vertical torsion angle. Contrary to the former system, it is not longer a precondition, that the elevator car is a rigid body or the manufacturing tolerances in very high buildings are almost zero. Therefore, the system presented is more realistic than its antecessor. The present paper describes the derivation of the additional torsion controller and compares the two unequal systems. Benefits and disadvantages of the augmented system are specified and evaluated.**

***Index Terms*— Electromagnetic actuator, elevator test bench, force decoupling, guideway transportation, linear guiding system, magnetic levitation (maglev), mechatronics, modeling, motion control, simulation**

I. Introduction

Nowadays, more and more high-rise buildings are constructed in Asia and other parts of the world. A high requirement to these buildings is the design of the traffic infrastructure within. The focus on improvements of the buildings' transportation systems rests on the elevator systems since the design of such a system for very high buildings is always a design near a technical threshold range. Additionally, new elevators have to be comfortable and have to possess low-maintenance.

A proposal for a faster but wear-resistant traffic system in high buildings is the employment of electromagnetic guides to elevators. These systems promise faster passenger transportation due to the frictionless operation and at least the same riding comfort as state of the art elevator systems due to the absent contact between slider and guide rail. In addition, these guideways have no consumption of lubricants, which is a further advantage compared to mechanical guideways. In former works (e.g. [1] and [2]), the assembling and operation of an elevator test bench is presented, which shows a well running system. The introduced system demonstrates an electromagnetic guiding system controlling five of the six spatial degrees of freedom (DOF) which are depicted in Figure 1. The elevator car is assumed to be a rigid body. It is fixed in one DOF by its propulsion device, which is a rope in this case. This is the DOF in vertical z-direction. The other five DOF are the translatory movements in x- and y-directions and the rotary movements α, β, and γ around the axes of a Cartesian coordinate system located at the center of gravity of the elevator car. A DOF control system is created to stabilize the elevator car. Measurements during the test bench operation show a good system response to disturbance forces. However, the assumption to behave like a rigid body seems to be not reasonable for an elevator car. Usually, elevator cars are manufactured in lightweight construction to minimize the entire mass, which has to be moved. This also counts for electromagnetic guided elevators. Thus, the elevator car will not behave like a rigid body and five DOF are not adequate to describe its spatial motion. The aim of the present work is to improve the electromagnetic guiding system by introducing a torsion controller that eliminates an angular deviation around the vertical z-axis of roof and floor of the elevator car. This deviation is described as a further DOF χ. The expectation of reducing displacement in this DOF is to lower the requirements to manufacturing tolerances of the

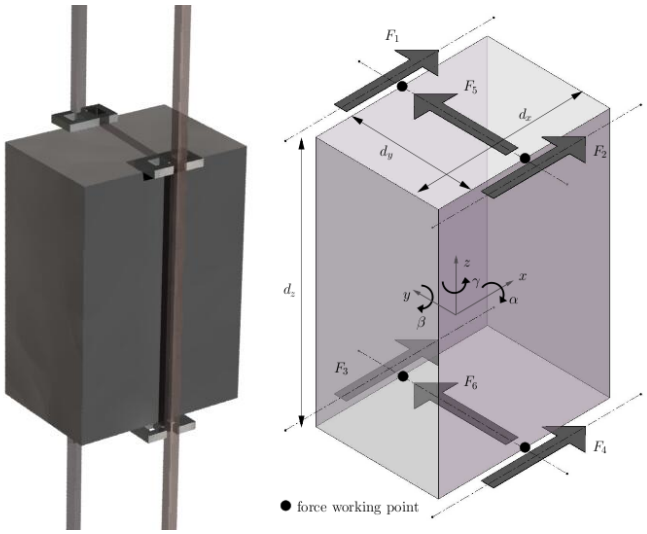

Fig. 1. Arrangement of the actuators on the elevator car (left hand side) as well as their actuating forces and the elevator's DOF (right hand side).

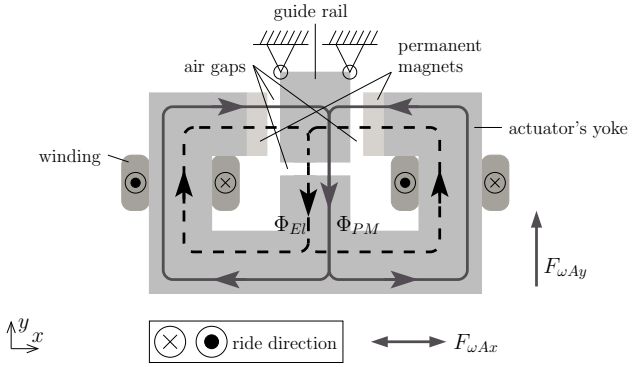

Fig. 2. Flux in an ω-actuator's cross-section.

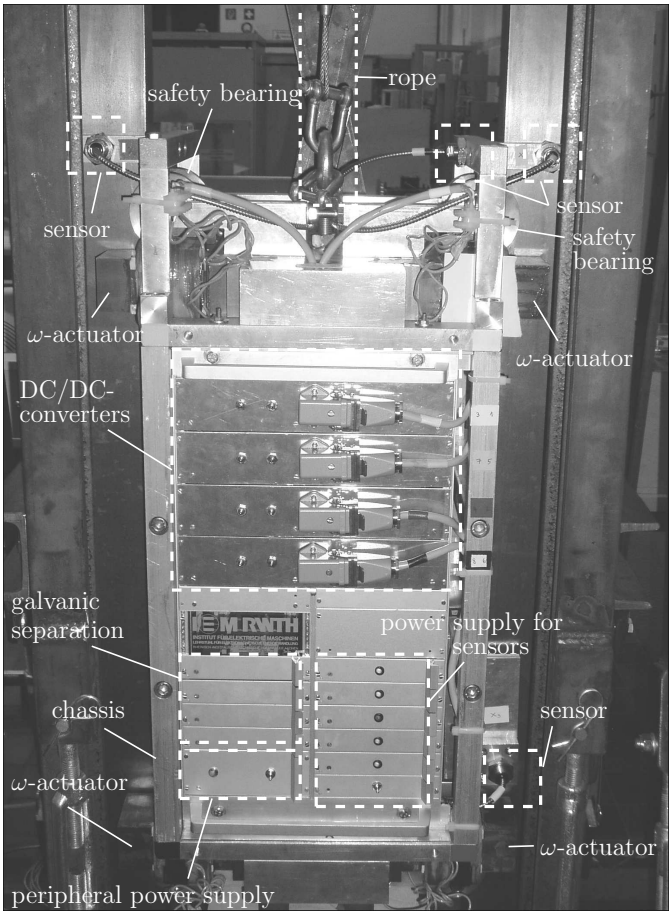

Fig. 3. Elevator test bench.

elevator's rails and of the elevator car.

II. Guiding Topology

A. Actuators

An important component of the guideway is the so called guiding shoe, which transmits disturbance forces from the elevator car to the guide rail. As aforementioned, conventional guiding shoes are constructed using rollers or slideways.

The electromagnetic alternative presented is the actuator in ω-shape [3]. This ω-actuator is an electromagnetic actuator able to excite three independent pulling forces. This is a significant improvement with respect to conventional u-shaped actuators [4], which generate a pulling force in one direction only. Therefore, one ω-actuator replaces three u-actuators. A further actuator is the magnet module presented in [5], which controls one complete DOF, i.e. producing a force in one direction (positive and negative). Nevertheless, the ω-actuator controls one and a half DOF. Therewith, two ω-actuators substitute three magnet modules.

Fig. 2 shows the cross-section of an ω-actuator. It consists of a three-armed iron yoke, mounted with permanent magnets on the outer pole surfaces, and coils around the lateral arms. The operation of this actuator is based on the superposition of a permanent magnet flux Φ_{PM} with an electrically excited flux Φ_{El}.

B. Complete System

The actuators are mounted on opposite edges of roof and floor of the elevator car, i. e. four ω-actuators are mounted on one car. In combination with two guide rails located on opposite walls of the elevator shaft, the complete guiding system is formed (Fig. 1). Altogether, the four ω-actuators produce twelve pulling forces, organised in pairs along six action lines. Hence, a total of six forces remain to control the position of the elevator car, i. e. to control all spatial degrees of freedom except the elevator's driving force. These forces are depicted in Fig. 1 as well. Fig. 3 presents a test bench of the electromagnetic guides elevator.

C. The Test System's Optimization Potential

In a first step, the stiffness of the chassis is assumed to be quite high (the compliance is assumed to be zero); a deformation due to the electromagnetic forces of the actuating electromagnets is not expected. Hence, it is assumed, that the measuring of five local positions is sufficient for a complete position determination of the elevator car. The five local positions measured are three times the actuators' air gaps in x-direction (at position of forces F_1, F_2, and F_3 corresponding to Fig. 1) and two times the air gaps in y-direction (at position of forces F_5 and F_6 corresponding to Fig. 1). The operation of this test bench demonstrates a running system, but an observing of the air gaps at the local position x_4 (at position of force F_4 in Fig. 1) reveals a deviation to the ideal position.

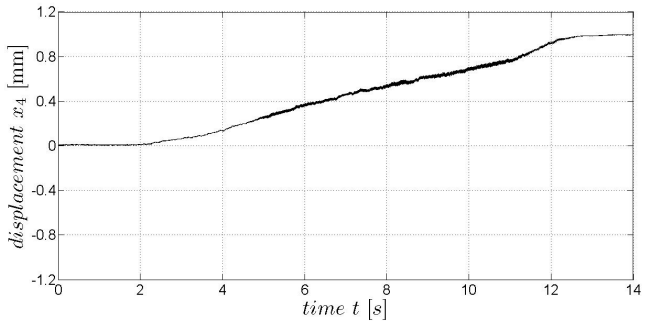

Fig. 4. Displacement of one actuator in x-direction measured by air gap sensor x_4 during the elevator's ride.

Fig. 4 presents the measured position x_4 during a ride of the elevator car from top to bottom of its shaft. It can be seen, that the the local actuator is not centered in its x-position but changes the value of its displacment during movement in z-direction. The other three actuators do not show this deviation when the elevator rides. This effect demonstrates that the elevator car is twisted and therefore not comparable to a rigid body or the manufacturing tolerances of the guide rails are higher than expected. However, the capturing of five sensor signals is not sufficient.

D. Utilizing the sixth sensor signal

In a first step, it is investigated, which influence on the existing system, containing five controlled DOF (5 DOF mode, as described in [6]), the capturing and utilizing of the additional x_4 sensor signal has. In [7] can be read, how the five DOF are calculated by five sensor signals. The calculation procedure is a coordinate transformation from the measured air gaps into the global DOF. To utilize the sixth sensor signal an augmented transformation matrix $\mathbf{T}$ is introduced:

$$\mathbf{T} = \begin{bmatrix} 1/4 & 0 & 1/4 & 1/4 & 0 & 1/4 \\ 0 & 1/2 & 0 & 0 & 1/2 & 0 \\ 0 & -1/d_z & 0 & 0 & 1/d_z & 0 \\ 1/2d_z & 0 & 1/2d_z & -1/2d_z & 0 & -1/2d_z \\ -1/2d_y & 0 & 1/2d_y & -1/2d_y & 0 & 1/2d_y \end{bmatrix}, \quad (1)$$

with d_y as the horizontal distance and d_z as the vertical distance between two ω-actuators. The coordinate transformation is performed as follows:

$$\mathbf{q} = \mathbf{T} \cdot \boldsymbol{\delta_{sensor}}, \quad (2)$$

where $\mathbf{q}$ is the position vector of the elevator car containing all five DOF

$$\mathbf{q} = (x\ y\ \alpha\ \beta\ \gamma)^T \quad (3)$$

and $\boldsymbol{\delta_{sensor}}$ is the vector of the six sensor signals

$$\boldsymbol{\delta_{sensor}} = (x_1\ y_1\ x_2\ x_3\ y_3\ x_4)^T. \quad (4)$$

However, this transformation matrix for utilizing the sensor signal x_4 is not the final solution. It can be seen, that $\mathbf{T}$ is a 6x5 matrix. Therefore, the DOF are exactly determined by the local air gap sensor signals, but on the other side there is an infinite number of solutions for the air gap heights by given DOF. The system is under-determined. This means, if all DOF are controlled to zero, the local air gaps need not to be in the central position. In theory, also an impact of the actuators on the guide rails is possible. The result of a system observed and controlled in the way described is presented in Fig. 5. It can be seen, that the four air gaps do not posses their reference value ($0\,\mathrm{mm}$), which would mean that the ω-actuators are staying in a central x-position around the guide rails. Instead of that, they are moving in every moment to the position, which provides the system's lowest energetic state. To avoid an undefined system behavior and to avoid the posibility of impacts a full defined system model has to be obtained.

E. DOF Augmentation

If the elevator test bench shall demonstrate a realistic elevator system, a sixth measured and controlled DOF is essential. Therefore, the elevator's torsion angle χ is introduced, which is calculated by the further augmented transformation matrix $\mathbf{T_{6D}}$:

$$\mathbf{T_{6D}} = \begin{bmatrix} 1/4 & 0 & 1/4 & 1/4 & 0 & 1/4 \\ 0 & 1/2 & 0 & 0 & 1/2 & 0 \\ 0 & -1/d_z & 0 & 0 & 1/d_z & 0 \\ 1/2d_z & 0 & 1/2d_z & -1/2d_z & 0 & -1/2d_z \\ -1/2d_y & 0 & 1/2d_y & -1/2d_y & 0 & 1/2d_y \\ -1/d_y & 0 & 1/d_y & 1/d_y & 0 & -1/d_y \end{bmatrix} \quad (5)$$

The coordinate transformation of the full determined system is performed as follows:

$$\mathbf{q_{6D}} = \mathbf{T_{6D}} \cdot \boldsymbol{\delta_{sensor}}, \quad (6)$$

where $\mathbf{q_{6D}}$ is the position vector of the elevator car containing all six DOF

$$\mathbf{q_{6D}} = (x\ y\ \alpha\ \beta\ \gamma\ \chi)^T. \quad (7)$$

Fig. 6 presents the resulting uncontrolled torsion angle during operation in 5 DOF mode. As presented, the angle χ is unequal to zero for the most time.

In addition to the augmented sensor signal transformation matrix, the force transformation matrix and the current transfomation matrix (introduced in [1]) have to be augmented as well.

The force transformation matrix, which transforms the local actuator forces into the global forces and torques, results as

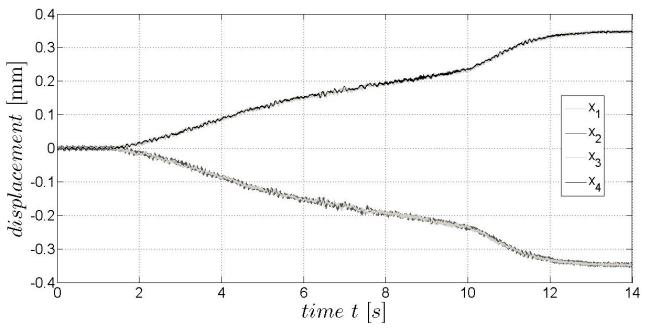

Fig. 5. The four measured signals of the air gaps in x-direction during the elevator's ride.

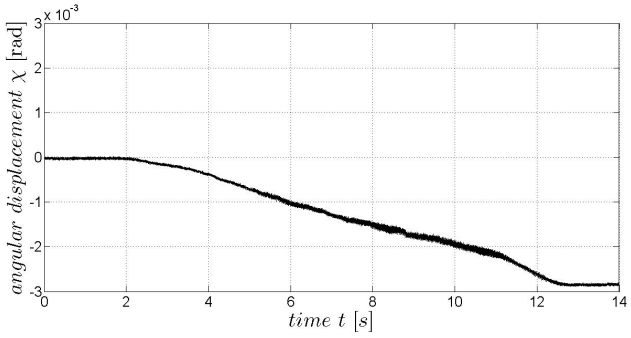

Fig. 6. Uncontrolled torsion angle χ calculated by the measurement results of four air gap sensors during the elevator's ride.

follows:

$$\begin{pmatrix} \tilde{F}_x \\ \tilde{F}_y \\ \tilde{M}_\alpha \\ \tilde{M}_\beta \\ \tilde{M}_\gamma \\ \tilde{M}_\chi \end{pmatrix} = \begin{bmatrix} 1 & 0 & 1 & 1 & 0 & 1 \\ 0 & 1 & 0 & 0 & 1 & 0 \\ 0 & -d_z/2 & 0 & 0 & d_z/2 & 0 \\ d_z/2 & 0 & d_z/2 & -d_z/2 & 0 & -d_z/2 \\ -d_y/2 & 0 & d_y/2 & -d_y/2 & 0 & d_y/2 \\ -d_y/2 & 0 & d_y/2 & d_y/2 & 0 & -d_y/2 \end{bmatrix} \begin{pmatrix} F_1 \\ F_5 \\ F_2 \\ F_3 \\ F_6 \\ F_4 \end{pmatrix} \tag{8}$$

Global values are tagged by the $\sim$-symbol. The here introduced sixth row describes the transformation from local forces (F_1, F_2, F_3, F_4, F_5, and F_6) to the torsional moment $\tilde{M}_\chi$. The current transformation matrix describes the transformation from virtual global quantities to local coil currents. Due to an augmention to an 8x8 matrix described in [1] the transformation for χ is still implemented, e.g. compare $\tilde{\Theta}_{h3}$ in [1] with $\tilde{I}_\chi$ below:

$$\begin{pmatrix} \tilde{I}_x \\ \tilde{I}_y \\ \tilde{I}_\alpha \\ \tilde{I}_\beta \\ \tilde{I}_\gamma \\ \tilde{I}_\chi \\ \tilde{I}_{h1} \\ \tilde{I}_{h2} \end{pmatrix} = \begin{bmatrix} 1 & -1 & -1 & 1 & 1 & -1 & -1 & 1 \\ 1 & 1 & -1 & -1 & 1 & 1 & -1 & -1 \\ -1 & -1 & 1 & 1 & 1 & 1 & -1 & -1 \\ 1 & -1 & -1 & 1 & -1 & 1 & 1 & -1 \\ -1 & 1 & -1 & 1 & -1 & 1 & -1 & 1 \\ -1 & 1 & -1 & 1 & 1 & -1 & 1 & -1 \\ 1 & 1 & 1 & 1 & 1 & 1 & 1 & 1 \\ 1 & 1 & 1 & 1 & -1 & -1 & -1 & -1 \end{bmatrix} \begin{pmatrix} I_{1l} \\ I_{1r} \\ I_{2l} \\ I_{2r} \\ I_{3l} \\ I_{3r} \\ I_{4l} \\ I_{4r} \end{pmatrix} \tag{9}$$

Based on these adjustments the control design is explaind in detail in the following section.

III. 6TH DOF CONTROL UNIT DESIGN

The former sections describe the necessity of a torsion controller. With an approval of a torsional deformation of the elevator car and with an observation of the tosion, a further equation to describe and model the system behavior has to be obtained. Due to a high torsional stiffnes around x-axis and y-axis and due to the larger dimensions of the elevator car in z-direction, only the torsianal deformation around the z-axis is analyzed

A. Torsion Equations

Before deriving the torsion's equations two important predefinitions are made:

- The main part of the mass is placed in the roof and the floor of the elevator's chassis.
- The roof and floor of the chassis are rigid. Thus, the compliance is located in the walls.

Due to these assumptions the torsion is modeled as a mass-spring oscillator [8] and the torsion is described by the angular torsion displacement between roof and floor.

$$\chi = \phi_{top} - \phi_{bottom}. \tag{10}$$

Roof and floor are comparable to the oscillating mass, the chassis' wall is comparable to the tosion's spring. Hooke's law delivers the oscillation differential equation

$$M_\chi - c \cdot \chi = J_\chi \ddot{\chi}, \tag{11}$$

with J_χ as the torsion oscillation's moment of inertia and c as the stiffness of the chassis. To define the stiffness of the chassis, an excurse to mechanics of materials is performed. The chassis' wall is idealized in its resistance contrary to an acting torsion moment as a hollow profile. That means, it is described as a thin-walled self contained cross-section. A torsional load is affiliated by shear that acts in this cross-section.
The twist of a profile with length h and under impact of the torsion moment M_T around the z-axis is defined as

$$\chi = \frac{M_T \cdot h}{G \cdot I_T}. \tag{12}$$

G is the shear module, which describes the characteristic of the material under a shear load, I_T is the tosion's moment of inertia, which describes the influence of the profile geometry on the torsional stiffness. According to this, the differential torsion equation is derived as follows:

$$M_\chi = J_\chi \ddot{\chi} + \frac{G \cdot I_T}{h} \cdot \chi. \tag{13}$$

B. Derivation of the State Space Equations

The derivation of the state space equations [9] for the spatial DOF is the same as described in [1], [7], and [2]. Therefore, in this section the derivation of the state space equations for the additional DOF χ is presented in detail.
The mathematical modeling bases on the deduced differential equations. The state variables are the angular position χ and the angular speed $\dot{\chi}$. These quantities are deviation quantities, this means they describe the deviation to the reference position and the reference speed respectively. To avoid a permanent deviation, the integral of the angular position $\int \chi dt$ is added to the state variables:

$$\boldsymbol{\chi} = \begin{pmatrix} \int \chi dt \\ \chi \\ \dot{\chi} \end{pmatrix}. \tag{14}$$

Equation 8 expresses the torsional moment with the local quantities of the guiding system, the corresponding air gaps. Including the applied torque and the linearized force equations follows

$$\tilde{M}_\chi(\Delta x_i) = d_y \cdot (-F_{\delta x} \cdot \Delta x_1 + F_{\delta x} \cdot \Delta x_2 + F_{\delta x} \cdot \Delta x_3 - F_{\delta x} \cdot \Delta x_4), \tag{15}$$

with Δx_i as the respective deviation to the desired air gap value and $F_{\delta x}$ as the linearization factor of the local forces in x-direction. After transformation to global quantities results

$$\tilde{M}_\chi(\chi) = d_y \cdot (d_y \cdot F_{\delta x} \cdot \chi). \tag{16}$$

With equation 13 for the angular acceleration follows

$$\ddot{\chi}(\chi) = \frac{1}{J_\chi} \cdot (d_y^2 \cdot F_{\delta x} - \frac{G \cdot I_T}{d_z}) \chi. \tag{17}$$

Due to the dependancy of the torsional moment on the coil currents (I_{1l} to I_{4r}) follows

$$\tilde{M}_\chi(I_i) = F_{Ixl} \cdot (I_{1l} + I_{2l} - I_{3l} - I_{4l}) + F_{Ixr} \cdot (I_{1r} + I_{2r} - I_{3r} - I_{4r}), \tag{18}$$

with F_{Ixl} and F_{Ixr} as further linearization factors of the local forces in x-direction.
The transformation to global quantities yields

$$\tilde{M}_\chi(\tilde{I}_\chi, \tilde{I}_{h2}) = F_{Ixl} \cdot (\frac{1}{2}\tilde{I}_\chi + \frac{1}{2}\tilde{I}_{h2}) + F_{Ixr} \cdot (-\frac{1}{2}\tilde{I}_\chi + \frac{1}{2}\tilde{I}_{h2}). \tag{19}$$

With $F_{Ixl} = -F_{Ixr}$ results

$$\tilde{M}_\chi(\tilde{I}_\chi) = F_{Ixl} \cdot \tilde{I}_\chi. \tag{20}$$

Finally, for the acceleration in dedendancy to current $\tilde{I}_\chi$ follows

$$\ddot{\chi}(\tilde{I}_\chi) = \frac{d_y^2}{J_\chi} \cdot F_{Ixl} \cdot \tilde{I}_\chi. \tag{21}$$

The state space equation of DOF χ results in

$$\underbrace{\begin{pmatrix} \chi \\ \dot{\chi} \\ \ddot{\chi} \end{pmatrix}}_{\dot{\boldsymbol{x}}} = \underbrace{\begin{bmatrix} 0 & 1 & 0 \\ 0 & 0 & 1 \\ 0 & \frac{d_y^2}{J_\chi} \cdot F_{\delta x} - \frac{G \cdot I_T}{d_z \cdot J_\chi} & 0 \end{bmatrix}}_{\mathbf{A}_{\boldsymbol{\chi}}} \cdot \underbrace{\begin{pmatrix} \int \chi dt \\ \chi \\ \dot{\chi} \end{pmatrix}}_{\boldsymbol{x}} + \underbrace{\begin{bmatrix} 0 \\ 0 \\ \frac{d_y^2}{J_\chi} \cdot F_{Ix} \end{bmatrix}}_{\mathbf{b}_{\boldsymbol{\chi}}} \cdot \underbrace{\tilde{I}_\chi}_{u} \tag{22}$$

and

$$y = \underbrace{(0 \quad 1 \quad 0)}_{\mathbf{c}_{\boldsymbol{\chi}}} \cdot \begin{pmatrix} \int \chi dt \\ \chi \\ \dot{\chi} \end{pmatrix}. \tag{23}$$

Here, $F_{\delta x}$ and F_{Ix} are linearization factors. These two equations are the description of the uncontrolled system. $\mathbf{A}_{\boldsymbol{\chi}}$ is the system matrix, $\mathbf{b}_{\boldsymbol{\chi}}$ the input vector, and $\mathbf{c}_{\boldsymbol{\chi}}$ the output vector. The feedthrough value d_χ is chosen to be zero, since there is no direct feedthrough in a real system. Here, y is the output value of the state space system and not the DOF y.

C. Control Parameters

Due to the eigenvalues located on the imaginary axis the system is instable. The eigenvalues are placed by feedback of the state space vector and combination with the input vector. For feedback the vector $\mathbf{k}$ is deployed, which contains a factor for each state variable. The controlled system is described as follows:

$$\dot{\boldsymbol{\chi}} = \mathbf{A}_{\boldsymbol{\chi}} \cdot \boldsymbol{\chi} + \mathbf{b}_{\boldsymbol{\chi}} \cdot u \tag{24}$$

$$u = -\mathbf{k} \cdot \boldsymbol{\chi}\ . \tag{25}$$

u is the input value, $\boldsymbol{\chi}$ is the state vector, and $\mathbf{k}$ is the feedback vector.
Both equations deliver the new system matrix $\mathbf{A}_\mathbf{k}$

$$\mathbf{A}_\mathbf{k} = \mathbf{A}_{\boldsymbol{\chi}} - \mathbf{b}_{\boldsymbol{\chi}} \cdot \boldsymbol{\chi}. \tag{26}$$

This augmented operation of the elevator guiding system with six controlled DOF is called 6 DOF mode.

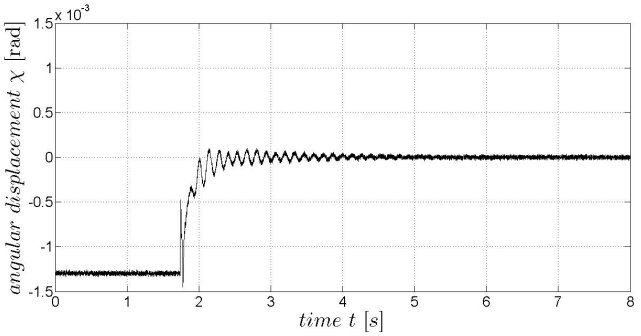

Fig. 7. Torsion angle χ calculated by the measurement results of four air gap sensors during switching the systems operation mode from five DOF control to six DOF control.

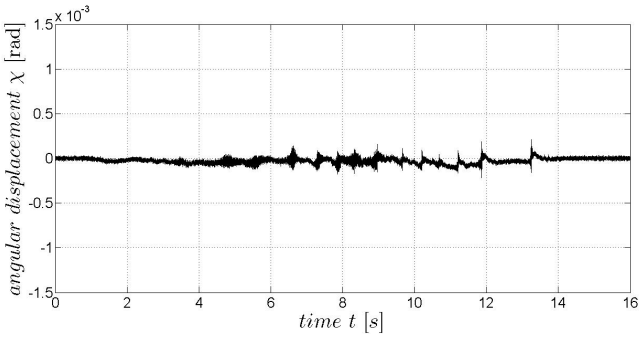

Fig. 8. Controlled torsion angle χ calculated by the measurement results of four air gap sensors during the elevator's ride.

IV. Measurements

In a first measurement, the elevator guiding system directly switches from 5 DOF mode to 6 DOF mode. Fig. 7 presents the switching process response of torsion angle χ. It can be seen, that the deviation to the desired value $\chi = 0$ amounts approximately $\Delta\chi = 1.5\,\mathrm{mrad}$ at time $t = 0\,\mathrm{s}$. The hard switching to 6 DOF mode occurs after approximately $t = 1.8\,\mathrm{s}$ measurement. The controlled variable χ shows fast motion to the desired value inclusive a transient oscillation, which lasts a few seconds. This oscillation depends on the control action of the other five DOF controllers. Every controller works completely independent, but influences each other in a real system. To avoid a disturbing of the five spatial DOF and to provide smooth and silent operation of the elevator car, the χ-controller is much slower than the other five controllers. Also during the elevator car's ride through the elevator shaft, the guiding system shows a robust system behavior in 6 DOF mode. Fig. 8 presents the torsion angle χ when the elvator car rides from top to bottom of its shaft. In difference to 5 DOF mode operation, presented in Fig. 6, χ remains on its reference position. Very small deviations are compensated quite fast. Furthermore, the ω-actuators remain in their desired position. This is evaluated by measuring the respective air gap lengths x_1, x_2, x_3 and x_4. The result, which shows the four air gap sensor signals during the whole ride in vicinity of reference value zero is shown in Fig. 9. It can be seen, that all actuators

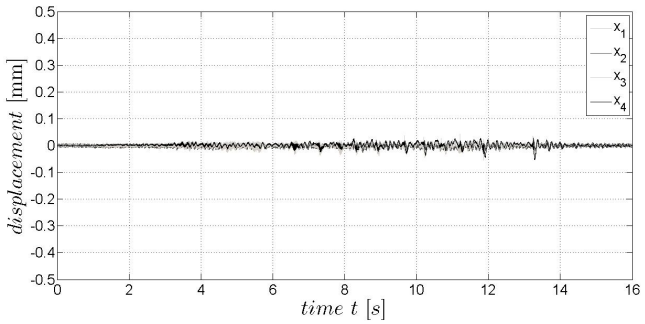

Fig. 9. The four measured signals of the air gaps in x-direction during the elevator's ride in 6 DOF mode.

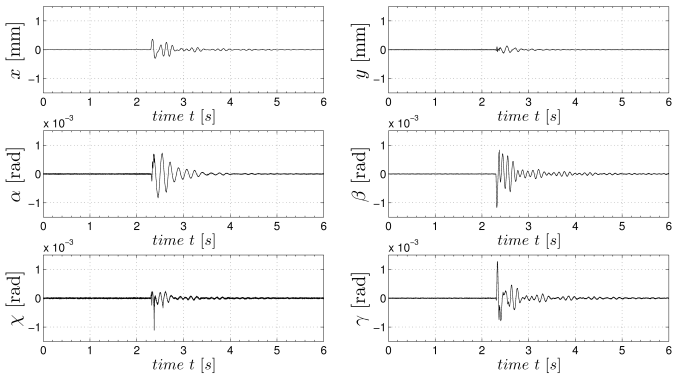

Fig. 10. The six measured DOF exited with an impulse in x-direction on the floor of the elevator's chassis.

stay in the desired central x-position around the guide rails ($x = 0$). The risk of an actuator's impact on the guide rails is averted.

In final measurements, the functionality of the entire guiding system in 6 DOF mode is investigated. During operation, the system is excited by external force impulses on the elevator car's chassis in several directions. As an example, the force impact in x-direction on the floor of the elevator car is presented. Fig. 10 shows the excitation response of all DOF. As displayed, all six DOF show an impact response and a fast disturbance compensation. However, that all DOF controllers show a reaction is a reasonable result. On the one hand, the force impulse was not exerted to the barycenter of the elevator car. Due to this, all spatial DOF are excited as well. Furthermore, the actuators moved out of their desired position. This produces additional magnetic forces to the actuators and herewith to the elevator car's chassis, which leads to a deformation (torsion) of the elevator car. After a period of $t \approx 1\,\mathrm{s}$ all DOF deviations are compensated and the DOF are back in their desired position. The entire system works similar to its antecessor system and the additional torsion controller has no negative influence to the control quality of the other five DOF controller.

V. Conclusion

A test bench for the validation of an electromagnetic guiding system for elevator cars is introduced. Advances of a contactless guided elevator system are detailed in the beginning. Thereafter, the design of the elevator test bench is explaind. Starting with the special kind of actuator implemented to the elevator car, the complete system setup is presented. After this, the disadvanteges of the actual state of system, described in former publications, are declared. These are the systems inability to compensate manufacturing tolerances as well as the unrealistic assumption to model the elevator car as a rigid body. The disadvantages of the former system are proven and illustrated by measurement results. It is shown, that a system augmentation from five DOF to six DOF may avoid the disadvatages presented.

Furthermore, an implementation of an additional torsion controller, to the guiding system for the compensation of manufacturing tolerances in realistic systems is described. An approach for the modeling of this additional DOF is exemplified as well. Subsequently, the derivation of the torsion controller is declared in detail.

Finally, the improved system behavior is depicted. Measurements of the air gap sensor signals as well as the new DOF χ shows a constant abidance on their reference position only in the new augmented control mode, the so-called 6 DOF mode. One measurement shows the entire system excited by external impacts in several directions. The system's response is investigated and it is demonstrated that the additional torsion controller only has a low influence to the other DOF controllers. Altogether, the measurement results show a robust state-space controller with a high control quality. The described disadvatages of the former system are compensated by the augmented guiding system.

References

[1] B. Schmülling, R. Appunn, and K. Hameyer, "Electromagnetic guiding of vertical transportation vehicles: state control of an over-determined system," in *XVIII International Conference on Electrical Machines*. Vilamoura, Portugal: ICEM, September 2008.

[2] R. Appunn, B. Schmülling, and K. Hameyer, "Electromagnetic guiding of vertical transportation vehicles: Experimental evaluation," *IEEE Transactions on Industrial Electronics*, vol. 57, no. 1, pp. 335–343, January 2010.

[3] M. Morishita and M. Akashi, "Electromagnetic non-contact guide system for elevator cars," in *The Third International Symposium on Linear Drives for Industry Applications*. Nagano, Japan: LDIA, October 2001, pp. 416–419.

[4] B. Schmülling, O. Effing, and K. Hameyer, "State control of an electromagnetic guiding system for ropeless elevators," in *European Conference on Power Electronics and Applications*. Aalborg, Denmark: EPE, September 2007, pp. 1–10.

[5] A. Schmidt, C. Brecher, and F. Possel-Dölken, "Novel linear magnetic bearings for feed axes with direct drives," in *International Conference on Smart Machining Systems at the National Institute for Standards and Technology*. Gaithersburg, MD, USA: www.smartmachiningsystems.com, March 2007.

[6] B. Schmülling, R. Appunn, F. Wikullil, and K. Hameyer, "Design and operation of an electromagnetically guided elevator test bench," in *The 7th International Symposium on Linear Drives for Industry Applications*. Incheon, Korea: LDIA, September 2009.

[7] B. Schmülling, *Elektromagnetische Linearführungen für Aufzugsysteme*. Aachener Schriftenreihe zur Elektromagnetischen Energiewandlung, Band 8: Shaker Verlag, 2009, Dissertation, RWTH Aachen University.

[8] D. J. Ewins, *Modal Testing: Theory, Practice and Application*. Baldock: Research Studies Press LTD., 2000.

[9] D. Li and H. Gutierrez, "Observer-based sliding mode control of a 6-dof precision maglev positioning stage," in *34th Annual Conference of Industrial Electronics*. Orlando, Florida, USA: IEEE IECON 2008, November 2008, pp. 2562–2567.